Stratified Shear Flow: Instability and Wave Radiation

B. R. Sutherland
Dept. Mathematical and Statistical Sciences, University of Alberta Edmonton, Canada

Abstract

The stability and evolution of a two-dimensional shear flow in nonuniformly stratified fluid is examined with a focus on investigating circumstances under which internal waves are excited. If the fluid is uniformly stratified, significant internal wave generation does not occur and the Kelvin-Helmholtz unstable flow evolves by wrapping up into coherent vortices on the scale of the wavelength of the most unstable mode. If the fluid above the shear is sufficiently more strongly stratified than the fluid spanning the mixing region then large amplitude internal waves are generated that extract significant momentum from the mean flow. The momentum transport and consequent drag induced on the mixing region is examined as a function of the strength of and distance from the region of increased stratification above the shear layer.

1 Introduction

A broad class of instability phenomena in fluid flows can be understood to occur as a result of resonant interactions between neutrally propagating waves. In uniform-density shear flows with weak viscosity, for example, Kelvin-Helmholtz (KH) instability occurs through coupling between two Rayleigh waves situated on either flank of a shear layer. Until nonlinear effects become important the waves grow exponentially in amplitude by drawing energy from the mean flow. Though a continuous spectrum of wave-pairs are unstable, typically one sees that the instability is dominated by the development of the pair with the fastest growth rate: the most unstable mode. The wavelength of this mode is proportional to the depth of the shear layer. The amplitude of the waves grow and ultimately develop into a string of vortices, or "billows", which may then go on to pair or to break down turbulently through three-dimensional effects. As a result of mixing, the shear-layer thickens and so may become unstable to disturbances of ever larger scale limited only by domain size or dynamics such as the "beta"-effect, which act on a planetary scale.

In a stratified shear flow, a greater variety of unstable motions are possible through the coupling of Rayleigh waves with internal waves. A Holmboe instability, for example, is the result of coupling between a Rayleigh wave on one flank of a shear-layer (in which flow speed changes with height) with an internal wave at a density interface that is offset from the shear-layer's mid-depth [1].

The nonlinear evolution of both stratified KH instabilities and Holmboe instabilities differ significantly from unstratified KH instability in that the mean flow kinetic energy that feeds their growth is partially siphoned-off as potential energy. Thus the shear layer can thicken to only a finite extent independent of domain size or other dynamics. Details of these processes are described in a recent review by Peltier and Caulfield [2].

Conversely, in a continuously stratified fluid, the evolution of a shear flow is not necessarily localized about the shear-layer; the instability can be detected far away if vertically propagating internal waves are generated.

The implications for such dynamics in geophysical fluid flows are profound. Not only can shear layers act as a dynamic source of internal waves in the atmosphere and ocean, but the evolution of the shear layer itself is significantly modified as a result of continuous energy and momentum extraction by internal waves. In particular, through transporting momentum vertically away from the shear layer, internal waves exert a drag on the mean flow where they are generated and they accelerate the mean flow at levels where they break.

Most investigations of shear generation of internal waves in the atmosphere have assumed a uniform background stratification surrounding a localised shear layer. Though the most unstable mode of KH instability does not directly excite internal waves in this circumstance [3, 4], it is possible for a modulation of instability to excite internal waves on scales much larger than the wavelength of the most unstable mode [5, 6, 7]. Another possibility is that internal waves can be generated when a shear-induced mixing region collapses [8].

In nonuniformly stratified fluid, it is possible for internal waves to be generated directly by KH instability [9, 10]. The condition for this to occur is characterised by the bulk Richardson numbers, J_0 and J_1, characterising the strength of the stratification within and outside the shear layer, respectively. Heuristically, one requires both that J_0 is sufficiently small (less than approximately $1/4$) for instability to occur and that J_1 is sufficiently large for the Doppler-shifted frequency of the most unstable mode to be less than the buoyancy frequency far from the mixing region.

Numerical simulations have shown that internal waves generated by this mechanism are so large that significant drag can be induced upon the mixing region [11, 10, 12] and that the waves themselves can transport momentum far from the source, even across the critical layer of a second nearby stably stratified shear layer [13].

One purpose of the work presented here is to review linear stability theory for stratified shear flows, in particular, those flows with piecewise-linear velocity and stratification profiles. This is done in section 2. In section 3, stability calculations are performed for several specific basic state profiles, which collectively illustrate the mechanisms for shear instability and wave excitation. The results of numerical simulations, presented in section 4, show that wave excitation predicted by linear theory does indeed result in significant wave generation and consequent drag due to the momentum loss from the shear layer. We summarize our results in section 5.

2 Linear theory

2.1 Derivation of Taylor-Goldstein equation

We examine exclusively the stability of a two-dimensional parallel flow, meaning that the ambient is characterised by density profile $\bar{\rho}(z)$ and horizontal wind $\bar{U}(z)$ that depend only upon the vertical co-ordinate z and not upon the horizontal direction x. The fluid is statically stable meaning that the density does not increase with height for any z. In such a flow, the background pressure is given by hydrostatic balance, $d\bar{p}/dz = -\bar{\rho}g$. That is, the pressure at height z is determined by the weight of fluid overlying z.

For atmospheric motions, rather than using $\bar{\rho}$, it is more appropriate to use "potential temperature" as a measure of the background stratification[14]. This quantity includes the combined effects of temperature and pressure to determine the effective density of a fluid parcel that, for example, adiabatically heats when it moves downward into higher pressure [14]. The dynamics discussed here are described equivalently by density variations in a liquid and by potential temperature variations in a gas. Therefore, we refer to the former more familiar quantity throughout this chapter.

We will be concerned with instability phenomena that occur on large enough scales that viscous effects are negligible but on small enough scales that density variations are important only as they affect buoyancy. The former assumption is excellent for most geophysical phenomena of interest. The latter assumption allows us to make the "Boussinesq approximation" in which the density field is treated as constant, ρ_0, everywhere in the equations of motion except in the buoyancy force term. This is an excellent approximation at all scales in the ocean and is applicable for atmospheric motions with vertical scales smaller than a few kilometers [15].

We represent perturbations to the background velocity, density and pressure fields by (u, w), ρ and p, respectively. Assuming these are small, the momentum conservation equations are

$$\frac{\partial u}{\partial t} + \bar{U}\frac{\partial u}{\partial x} + w\frac{d\bar{U}}{dz} = -\frac{1}{\rho_0}\frac{\partial p}{\partial x}, \tag{1}$$

$$\frac{\partial w}{\partial t} + \bar{U}\frac{\partial w}{\partial x} = -\frac{1}{\rho_0}\frac{\partial p}{\partial z} - \frac{1}{\rho_0}\rho g. \tag{2}$$

A consequence of the Boussinesq approximation is that the fluid is incompressible. This and the condition for mass conservation (the continuity equation) therefore give

$$\frac{\partial \rho}{\partial t} + \bar{U}\frac{\partial \rho}{\partial x} = -w\frac{d\bar{\rho}}{dz}, \tag{3}$$

$$\frac{\partial u}{\partial x} + \frac{\partial w}{\partial z} = 0. \tag{4}$$

Together these form four linear partial differential equations in the four unknown perturbation fields. Note that eqn (4) allows us to define a streamfunction ψ that satisfies $u = -\partial\psi/\partial z$ and $w = \partial\psi/\partial x$. This reduces our problem to one with three equations in three unknowns.

With straightforward manipulation we could reduce our problem to a single partial differential equation in one variable. However, it is easier to first simplify the coupled equations by exploiting the fact that the coefficients in the equations involve only z. The invariance in x and t allows us to substitute each field $f(x, z, t)$ by $\hat{f}(z)\exp[\imath(kx - \omega t)]$. The procedure is similar to a Fourier transform, in which case $\hat{f}$ would represent the z-dependent envelope of a disturbance with horizontal wavenumber k and frequency ω. Our substitution is more general, however, because both k and ω can be complex numbers. Thus, for example, the real part of ω denotes the disturbance frequency and the imaginary part denotes the growth rate. The quantity $\hat{f}(z)$ is referred to as the disturbance amplitude.

Making the substitutions in eqns. (1) and (2) gives, respectively,

$$\imath k(\bar{U} - c)\hat{u} + \hat{w}\frac{d\bar{U}}{dz} = -\frac{\imath k}{\rho_0}\hat{p}, \tag{5}$$

$$\imath k(\bar{U} - c)\hat{w} = -\frac{1}{\rho_0}\frac{d\hat{p}}{dz} - \frac{1}{\rho_0}\hat{\rho}g. \tag{6}$$

Here we have defined $c = \omega/k$, which is the horizontal phase speed of the disturbance. We eliminate $\hat{p}$ in these equations by taking the z derivative of eqn (5) and subtracting $\imath k$ times eqn (6). Effectively, this computes the prognostic equation determining the amplitude of the y-component of the vorticity, $\zeta = u_z - w_x$. Using eqn (4), we can write the components of velocity in terms of the streamfunction amplitude: $\hat{u} = -d\hat{\psi}/dz$ and $\hat{w} = \imath k\hat{\psi}$. Thus we have

$$-(\bar{U}-c)\left(-k^2+\frac{d^2}{dz^2}\right)\hat{\psi}+\hat{\psi}\frac{d^2\bar{U}}{dz^2}=\frac{g}{\rho_0}\hat{\rho}. \tag{7}$$

The amplitude equation from eqn (3) becomes

$$(\bar{U}-c)\hat{\rho}=-\hat{\psi}\frac{d\bar{\rho}}{dz}. \tag{8}$$

Finally, we eliminate $\hat{\rho}$ by taking g/ρ_0 times eqn (8) and adding $(\bar{U}-c)$ times eqn (7). Rearranging the result gives the famous "Taylor-Goldstein equation" [16]:

$$\frac{d^2\hat{\psi}}{dz^2}+\left[\frac{N^2}{(\bar{U}-c)^2}-\frac{\bar{U}''}{(\bar{U}-c)}-k^2\right]\hat{\psi}=0. \tag{9}$$

Here we have defined $N^2 = -(g/\rho_{00})d\bar{\rho}/dz$. N, which has units of inverse time, is known as the buoyancy frequency (also the "Brunt-Väisälä" frequency). As we demonstrate below, N is the frequency (in radians per unit time) associated with vertical oscillations of a stationary, uniformly stratified fluid.

2.2 Linear stability theory

For given background profiles of $N^2(z)$ and $U(z)$, the Taylor-Goldstein equation is an eigenvalue problem. That is, disturbances of horizontal wavenumber k must have vertical structure prescribed by eigenfunctions $\hat{\psi}$, nontrivial solutions of eqn (9), with corresponding eigenvalues $c(k)$. Using the definition $c = \omega/k$, the eigenvalues give us the dispersion relation $\omega \equiv \omega(k)$.

The Taylor-Goldstein equation is singular in the sense that the coefficients of the ordinary differential equation become infinitely large at critical levels $z \equiv z_c$ where $c = \bar{U}(z_c)$. In such circumstances, the eigenvalue problem may admit solutions where c, and hence ω, is complex-valued for some range of k. For each such eigenvalue, its complex conjugate is also an eigenvalue. Thus, for example, we can write $\omega(k) = \omega_0 \pm \imath\sigma$, in which ω_0 is the real part of the frequency and $\pm\sigma$ is the imaginary part of the complex conjugate pair of solutions. Without loss of generality, we suppose $\sigma > 0$. Recalling that $\psi(x,z,t) = \hat{\psi}\exp[\imath(kx-\omega t)] = \hat{\psi}\exp[\imath(kx-\omega_0 t)]\exp(\pm\sigma t)$, we see that complex eigenvalue solutions correspond to exponentially growing and decaying modes.

The essence of linear stability theory is to assess whether complex eigenvalue solutions exist for any k and, if so, to determine for what k the growth rate, σ, is largest. This is called the "most unstable mode" and corresponds to the instability one would expect to see emerge out of a background flow with superimposed random noise. The structure of the corresponding eigenfunction reveals how the instability grows at the expense of energy extracted from the background flow.

Thanks to a result by Miles [17], we know that all solutions of the Taylor-Goldstein equation have pure real eigenvalues (corresponding to all modes being stable) if the "gradient Richardson number" $\mathrm{Ri}_g \equiv N^2/(\bar{U}')^2$ is everywhere greater than or equal to 1/4.

Howard [18] elaborated upon Miles' result with his "semi-circle theorem", which states that the complex eigenvalue $c \equiv c_r + \imath c_i$ of unstable modes must satisfy

$$|(c_r - \langle \bar{U} \rangle) + \imath c_i| \leq \Delta\bar{U}/2 \tag{10}$$

in which $\langle \bar{U} \rangle = [\max(\bar{U}) + \min(\bar{U})]/2$ and $\Delta\bar{U} = \max(\bar{U}) - \min(\bar{U})$. For stratified flows this result holds only if N^2 is everywhere non-negative [16].

In particular, if $\bar{U} = U_0$ is constant, the inequality requires $c_i = 0$. Hence uniform flows must be stable. If $\bar{U}$ is not constant, the criterion (10) requires that the horizontal phase speed, c_r, of unstable modes lie between $\max(\bar{U})$ and $\min(\bar{U})$, a result first predicted by Rayleigh.

2.3 Piecewise-linear theory

It is often revealing to study the stability of flows prescribed by $\bar{U}$ and $\bar{\rho}$ that are piecewise-linear functions. Such flows are characterised by regions of uniformly stratified, uniform shear flows separated by discrete levels z where $\bar{U}$, $\bar{U}'$ (the z-derivative of $\bar{U}$) and/or $\bar{\rho}$ are discontinuous. If one further requires $N^2 = 0$ where $\bar{U}$ is non-constant, the Taylor-Goldstein equation simplifies to the simple ordinary differential equation

$$\frac{d^2\hat{\psi}}{dz^2} + \gamma^2\hat{\psi} = 0, \tag{11}$$

in which $\gamma^2 = -k^2$ in regions where $N^2 = 0$ and $\gamma^2 = {N_0}^2/(U_0 - c)^2 - k^2$ in regions where $N^2 = {N_0}^2$ and $\bar{U} \equiv U_0$ are constant.

The solution of eqn (11) gives either exponential or sine-cosine solutions depending on whether γ^2 is negative or positive, respectively.

The solutions found in each constant-shear and constant-N^2 region are matched across discontinuities of the background profiles by requiring continuity of vertical velocity and pressure. The first of these conditions requires continuity of

$$\frac{1}{\bar{U} - c}\hat{\psi}, \tag{12}$$

and the second requires continuity of the quantity

$$\bar{\rho}\left\{(\bar{U} - c)\frac{d\hat{\psi}}{dz} - \bar{U}'\hat{\psi} - \frac{g}{\bar{U} - c}\hat{\psi}\right\}. \tag{13}$$

In special cases in which the background density varies continuously across a particular boundary, the second condition simplifies to requiring continuity of $(\bar{U} - c)\hat{\psi}' - \bar{U}'\hat{\psi}$.

In problems involving $n+1$ regions separated by n levels where the background profiles are discontinuous, the general solutions of eqn (11) have $2(n+1)$ arbitrary constants associated with them. The matching conditions (13) and (12) relate these constants through $2n$ equations.

To close the problem, boundary conditions must also be imposed below the bottom level and above the top level. If the domain is bounded by a rigid boundary one insists that $\hat{w} = 0$ or, equivalently, $\hat{\psi} = 0$ at the boundary. If the domain is unbounded then two possibilities exist. If the fluid is unstratified in the unbounded region, then the general solution of eqn (11) gives increasing and decreasing exponentials and one keeps only the solution that is bounded. If the fluid is stratified and unsheared in the unbounded region, then eqn (11) gives upward- and downward-propagating wave solutions. Invoking causality, one keeps only the solution that propagates outward to infinity.

Together, the matching and boundary conditions constitute $2(n+1)$ equations in the $2(n+1)$ unknown coefficients of the general solutions in each of the $n+1$ layers. The differential equation eigenvalue problem is thus reduced to a matrix eigenvalue problem.

In the next section we will consider a number of special cases that serve to demonstrate how piecewise linear theory can give insights into the instability of flow with more complex stratification.

3 Examples of piecewise-linear problems

A broad class of flows become unstable as a consequence of resonant coupling between pairs of neutrally propagating waves. We will illustrate this in a sequence of examples.

3.1 Internal gravity waves

Here we consider the solution of the Taylor-Goldstein equation in the case $N^2(z) = {N_0}^2$ and $\bar{U}(z) = U_0$, both constants.

Thus we find solutions $\hat{\psi}(z) = C_+ \exp(\imath\gamma z)$ and $C_- \exp(-\imath\gamma z)$ in which γ plays the role of the vertical wavenumber m given explicitly by

$$m = \pm\gamma = \pm k\sqrt{\frac{{N_0}^2}{\Omega^2} - 1}. \tag{14}$$

Arbitrarily we have set γ to be the positive square root and we have defined $\Omega = \omega - U_0 k$, representing the Doppler-shifted frequency of the waves.

Rearranging eqn (14) gives the well-known dispersion relation for internal gravity waves:

$$\Omega^2 = {N_0}^2 \frac{k^2}{k^2 + m^2} \equiv {N_0}^2 \cos^2\Theta. \tag{15}$$

Here Θ is the angle to the horizontal in wavenumber space of the wavenumber vector. Equivalently, Θ is the angle to the vertical formed by lines of constant phase associated with the waves.

One of the consequences of the dispersion relation is that the vertical group velocity, $c_{gz} = \partial\Omega/\partial m$, is positive if m is negative and *vice-versa* (*e.g.* see Gill [14] §6). This observation will be important below in setting boundary conditions in unbounded domains.

Another consequence of eqn (15) is that Ω can be no larger than N_0 to have propagating wave solutions. Indeed, if the Doppler-shifted frequency exceeds the buoyancy frequency, then γ in eqn (14) must be pure-imaginary, which corresponds to exponential solutions for $\hat{\psi}$. Waves with this structure are said to be "evanescent", terminology borrowed from optics. A wave whose amplitude increases or decreases exponentially with height cannot exist on its own in an unbounded domain because its amplitude would become infinitely large in the limit of infinitely large either positive or negative z. However, we demonstrate below that evanescent waves can be manifest as segments within a piecewise-linear solution.

3.2 Trapped internal gravity waves

We now consider the moderately more complicated case of waves in a stationary fluid whose stratification is prescribed by

$$N^2 = \begin{cases} {N_0}^2 & |z| \le H \\ 0 & z > H. \end{cases} \tag{16}$$

We are particularly interested in long waves ($\hat{k} \equiv kH \ll 1$) that have the structure of interfacial waves in a two-layer fluid in the limit $H \to 0$. We therefore assume solutions to eqn (11) of the form

$$\hat{\psi} = \begin{cases} A_1 e^{-kz} & z > H \\ A_2\cos(\gamma z) + B_2 \sin(\gamma z) & |z| \le H \\ B_3 e^{kz} & z < -H, \end{cases} \tag{17}$$

in which γ is defined as in eqn (14).

Nontrivial solutions are given implicitly as a function of $\hat{k}$ by nondimensional values $\tilde{\gamma} \equiv \gamma/k$ satisfying

$$\frac{1}{\tilde{\gamma}} = \tan(\hat{k}\tilde{\gamma}) \tag{18}$$

In the limit $\hat{k} \to \infty$, the roots with the simplest vertical structure have $\tilde{\gamma} \sim \hat{k}^{-1/2}$. Rearranging, this gives the dispersion relation

$$\omega^2 \sim \frac{\hat{k}}{1+\hat{k}} {N_0}^2 \sim g'k, \tag{19}$$

which is indeed the dispersion relation for an interfacial wave in a two-layer fluid with infinite upper- and lower-layer depths and with density difference between the two layers given in terms of the reduced gravity $g' = g(\Delta\rho)/\rho_0$.

The amplitude of the horizontal velocity field corresponding to the eigenvalue represented by eqn (18) is

$$\hat{u} = A_\xi \omega \begin{cases} \cos(\hat{k}\tilde{\gamma})e^{\hat{k}(1-z/H)} & z > H \\ \tilde{\gamma}\sin(\tilde{\gamma}z/H) & |z| \le H \\ -\cos(\hat{k}\tilde{\gamma})e^{\hat{k}(1+z/H)} & z < H, \end{cases} \tag{20}$$

in which A_ξ is the maximum vertical displacement at $z = 0$.

We see that long waves introduce shear across the stratified layer. It is natural to ask under what circumstances the shear will be so strong that the layer will become dynamically unstable. To this end we compute the maximum value of the gradient Richardson number at $z = 0$:

$$\mathrm{Ri}_g = {N_0}^2/|\hat{u}'(0)|^2 = \frac{1}{(A_\xi k)^2}\frac{{N_0}^2}{\omega^2}\left(\frac{\omega^2}{{N_0}^2 - \omega^2}\right)^2 \simeq \frac{kH}{(A_\xi k)^2}.$$

In this last approximation we have taken the long-wave limit.

Immediately we notice that Ri_g is independent of ${N_0}^2$ in this limit. Thus increasing the stratification alone does not make the wave-induced flow more stable because there is a corresponding increase in the square of the maximum shear. For fixed kH, the only parameter that determines whether or not the stratified shear is stable is the amplitude. Specifically, the flow is stable if $A_\xi k < 2(kH)^{1/2}$.

3.3 Rayleigh waves

We now consider a uniform fluid ($N^2 = 0$) with a kinked-shear flow profile in an unbounded domain given by

$$\bar{U} = \begin{cases} 0 & z \ge 0 \\ s_0 z & z < 0. \end{cases} \tag{21}$$

Requiring bounded solutions to eqn (11), we find

$$\hat{\psi} = \begin{cases} Ae^{-kz} & z \ge 0 \\ Be^{kz} & z < 0. \end{cases} \tag{22}$$

The matching conditions, eqns. (12) and (13), applied at $z = 0$ give the simultaneous equations written in matrix form:

$$\begin{pmatrix} 1 & -1 \\ ck & ck + s_0 \end{pmatrix}\begin{pmatrix} A \\ B \end{pmatrix} = \begin{pmatrix} 0 \\ 0 \end{pmatrix}. \tag{23}$$

This matrix eigenvalue problem has nontrivial solutions if the determinant of the 2x2 matrix is zero. That is, if $2ck + s_0 = 0$.

Thus we have determined the dispersion relation for Rayleigh waves. Their horizontal phase speed varies with k according to

$$c = -s_0/(2k). \tag{24}$$

Because c is always real, we have shown that the kinked-shear profile is stable. Rearranging eqn (24) gives the dispersion relation expressed in nondimensional form by

$$\tilde{\omega} = -1/2, \tag{25}$$

where $\tilde{\omega} = \omega/s_0$.

The corresponding eigenvectors give the relative values of the amplitudes A and B above and below $z = 0$, respectively. The eigenfunctions themselves are exponentially decreasing functions about $z = 0$ and so, unlike internal waves, Rayleigh waves are not vertically propagating. They are interfacial waves that become more tightly concentrated about $z = 0$ as k increases and their horizontal extent becomes smaller. Correspondingly, we see that the phase speed of the Rayleigh waves always matches the speed of the background flow at some vertical level below $z = 0$, and this speed more closely matches the flow speed at $z = 0$ as k increases.

Indeed, by changing to a moving frame of reference, it is a simple matter to show that the phase speed of Rayleigh waves in a kinked-shear flow profile given by $\bar{U} + U_0$, with $\bar{U}$ defined in eqn (21), is $c = U_0 - s_0/(2k)$.

3.4 Kelvin-Helmholtz instability

We now demonstrate that the well known Kelvin-Helmholtz (KH) instability is the result of resonant coupling between pairs of Rayleigh waves. We consider a uniform fluid ($N^2 = 0$) with a shear flow profile given by

$$\bar{U} = \begin{cases} -U_0 & z \geq L \\ -U_0 z/L & |z| < L \\ U_0 & z \leq -L \end{cases} \tag{26}$$

This velocity profile is effectively the result of splicing together two kinked-shear flow profiles. For relatively short wavelength disturbances, we expect waves on one flank of the shear will not “see” the other flank. That is, disturbances should have the same dispersion relation as Rayleigh waves in the limit $kL \to \infty$.

Requiring bounded solutions to eqn (11), we find

$$\hat{\psi} = \begin{cases} Ae^{-kz} & z \geq L \\ B_1 \sinh kz + B_2 \cosh kz & |z| < L \\ Ce^{kz} & z \leq -L \end{cases} . \tag{27}$$

Note, the solutions in the middle region have been written in terms of hyperbolic functions in order to take advantage of symmetry.

Applying the matching conditions at $z = \pm L$ gives four equations in the four unknowns A, B_1, B_2 and C. After substantial algebraic manipulations one finds the eigenvalues $c(k)$ are given by

$$c^2 = \frac{{U_0}^2}{(2kL)^2}\left[(1-2kL)^2 - e^{-4kL}\right] \tag{28}$$

The corresponding dispersion relation, written in nondimensional form is

$$\tilde{\omega}^2 = \frac{1}{4}\left[(1-2\tilde{k})^2 - e^{-4\tilde{k}}\right], \tag{29}$$

in which $\tilde{k} = kL$ and, equivalent to our definition for Rayleigh waves, $\tilde{\omega} = \omega L/U_0$.

In the limit $\tilde{k} \to \infty$, $\tilde{\omega} \to \pm 1/2$, which, as we anticipated, is the dispersion relation for Rayleigh waves on the upper and lower flanks of the shear layer corresponding to the $-$ and $+$ sign, respectively.

Long wavelength disturbances on either flank are not independent of each other and, indeed, may resonantly couple to form growing modes with zero phase speed. This occurs whenever $\tilde{k} \lesssim 0.64$, in which case $\tilde{\omega}$ is a pure imaginary number. The fastest-growing mode occurs for a finite wavenumber, which is found to be $\tilde{k}^\star \simeq 0.398$, for which the growth rate is $\tilde{\omega}_i^\star \simeq 0.20$ (*e.g.* see Drazin and Howard [19] section II).

In a frame of reference moving with the speed of the fluid above $z = L$, the nondimensional (Doppler-shifted) frequency of this mode is $\tilde{\Omega}_r^\star = \tilde{k}^\star \simeq 0.398$.

3.5 Rayleigh-internal wave instability in stratified fluid

A stratified fluid, one whose density decreases with height, can support internal waves in addition to Rayleigh waves. As a consequence, coupling between these waves may give rise to instability, which we refer to here as Rayleigh-Internal Wave (RI) instability.

To demonstrate this, we consider the kinked-shear velocity profile given by eqn (21) in a non-uniformly stratified fluid that has constant density in the shear region and whose density decreases linearly with height beyond a distance H above the shear region. In terms of the squared buoyancy frequency this structure is prescribed by

$$N^2 = \begin{cases} {N_0}^2 & z \geq H \\ 0 & z < H. \end{cases} \tag{30}$$

We require bounded solutions and, if propagating waves exist above $z = H$, we require causality so that the waves move upward (away from the shear) not downward (in from infinity). This amounts to requiring that the vertical wavenumber of the internal waves is negative. Thus we assume

$$\hat{\psi} = \begin{cases} Ae^{-\gamma z} & z \geq H \\ B_1 e^{kz} + B_2 e^{-kz} & 0 \leq z < H \\ Ce^{kz} & z < 0, \end{cases} \tag{31}$$

in which $\gamma = k(1 - {N_0}^2/(ck)^2)^{1/2}$. The positive square root is taken if $ck \geq N_0$. If $ck < N_0$, the branch cut is taken so that $\gamma = \imath k({N_0}^2/(ck)^2 - 1)^{1/2}$. In this latter case γ plays the role of the vertical wavenumber for propagating internal waves, as can be seen from eqn (15). In eqn (31) The negative sign in the exponent of $\hat{\psi}$ for $z > H$ ensures upward propagating waves alone are considered.

Applying the matching conditions at $z = 0$ and $z = H$ gives four equations in four unknowns. The eigenvalues for this problem give the dispersion relation that, in nondimensional form, are roots of the cubic polynomial

$$\tilde{\omega}^3 + \frac{1}{2}\tilde{\omega}^2\left(1 + Je^{2\hat{k}}\right) + \frac{1}{2}J\tilde{\omega}\left(e^{2\hat{k}} - 1\right) + \frac{1}{2}J\sinh^2(\hat{k}), \tag{32}$$

in which $\hat{k} = kH$ and $J = {N_0}^2H^2/U^2$ is the bulk Richardson number.

In the case $J = 0$ we recover the dispersion relation for Rayleigh waves together with two zero roots. For J positive, the root corresponding to Rayleigh waves continues to be real valued. However, the two zero roots split to give complex-valued frequencies (hence unstable modes) for a range of H.

The domain of stability is shown in Figure 1, which plots contours of the frequency and (in unstable cases) the growth rate as a function of J and $\hat{k}$. For $J > 0$ the flow is unstable to all modes with $0 < \hat{k} < \ln(3)$. For $\hat{k} = \ln(3)$, marginally stable modes exist for $J = 1/3$. For larger $\hat{k}$, stable modes exist for a finite range of J. In the limit $\hat{k} \to \infty$, modes are stable with $0 \leq J \leq 1/4$.

Unlike the modified Rayleigh modes, which have nondimensional (real) frequency $\tilde{\omega}_r \simeq -(1+J)/2$ in the limit $\hat{k} \to 0$, the unstable modes have zero frequency in this limit. Indeed, singular perturbation theory reveals that in the limit $J \to \infty$ the dispersion relation of the unstable modes is

$$\tilde{\omega} \simeq e^{-\hat{k}}\sinh(\hat{k})\left(-1 + \imath e^{-2\hat{k}}/\sqrt{J}\right). \tag{33}$$

In this limit the most unstable mode occurs for wavenumbers satisfying $e^{2\hat{k}} \simeq 2$, (*i.e.* $\hat{k} \simeq 0.35$), in which case $\tilde{\omega} \simeq -1/4 + \imath(1/8\sqrt{J})$.

In the limit of small J we estimate the characteristics of the most unstable modes from two different perturbation expansions. In the limit $\epsilon \equiv Je^{2\hat{k}} \to$

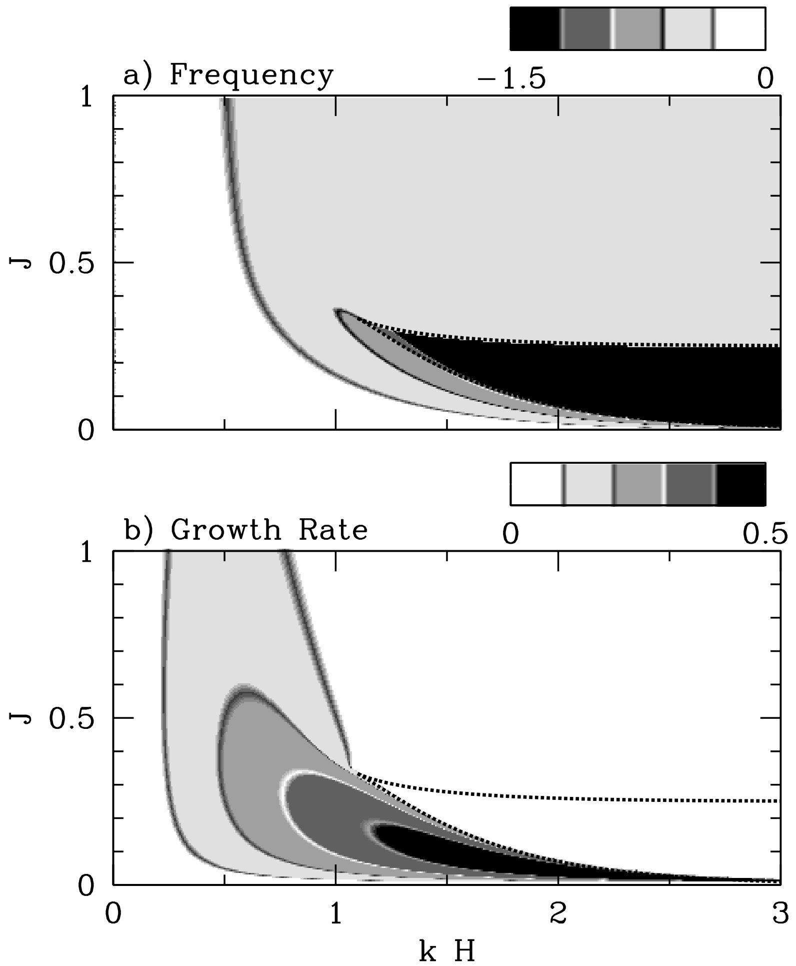

Figure 1: Contours of a) frequency and b) growth rate of RI modes given as a function of stratification, J, and nondimensional wavenumber, kH. The dashed curves in a) and b) denote the marginal stability boundary.

0, the dispersion relation of the unstable modes is

$$\tilde{\omega} \simeq [-\frac{1}{4}\epsilon + O(\epsilon^4)] + \imath\sqrt{\epsilon}\left(\frac{1}{2} - \frac{1}{16}\epsilon - \frac{1}{256}\epsilon^2\right). \tag{34}$$

The most unstable mode occurs for $\epsilon = 2$ (within the estimated radius of convergence).

Conversely, expanding about the lower branch of the neutral stability curve where $Je^{2\hat{k}} \simeq 4$ and $\tilde{\omega} \simeq -1$, we define $\epsilon \equiv 4 - Je^{2\hat{k}}$ and find

$$\tilde{\omega} \simeq [-1 + \frac{1}{4}\epsilon + O(\epsilon^4)] + \imath\sqrt{\epsilon}\left(\frac{1}{2} - \frac{1}{16}\epsilon - \frac{1}{256}\epsilon^2\right).$$

Again, we find the most unstable mode occurs for $\epsilon = 2$.

Thus, for small J, the most unstable mode occurs for wavenumbers satisfying $Je^{2\hat{k}} = 2$, in which case $\tilde{\omega}^\star \simeq -1/2 + \imath(23\sqrt{2}/64)$.

The fact that the nondimensional (real) frequency of the most unstable modes is the same as that for unmodified Rayleigh waves (which do not feel the effect of the stratification) is an indication that the instability results from Rayleigh-internal wave coupling to disturbances in the stratified fluid. These are not necessarily vertically propagating internal waves; for $J \ll 1$, the frequency of the most unstable mode is greater than the buoyancy frequency ($|\tilde{\omega}_r^\star/\sqrt{J}| = 1/2\sqrt{J} \gg 1$). However, in the limit of large J, the most unstable mode couples directly with vertically propagating waves with (nondimensional) horizontal wavenumber $\hat{k} \simeq 0.35$, frequency $|\tilde{\omega}_r^\star/\sqrt{J}| = 1/4\sqrt{J}$. growth rate $\tilde{\omega}_i^\star = 1/8\sqrt{J}$.

Below these are compared with the characteristics of the most unstable of KH instability.

3.6 Kelvin-Helmholtz instability in stratified fluid

The influence of uniform stratification ($N^2 = {N_0}^2$) on the instability of a shear layer has been well studied (*e.g.* see Drazin and Reid [16] §44). Consistent with Miles' stability criterion [17], a stratified shear layer is unstable only if the gradient Richardson number always exceeds 1/4. In particular, marginally stable eigenmodes of the hyperbolic-tangent shear layer ($\bar{U} = U_0 \tanh(z/L)$ occur for nondimensional wavenumbers $\tilde{k}$ satisfying $J = \tilde{k}^2(1-\tilde{k}^2)$, in which $J = {N_0}^2/(U_0/L)^2$ and $\tilde{k} = kL$ [20]. As J increases from 0 to 1/4, the wavenumber and (real) frequency of the most unstable mode hold approximately constant values, while the growth rate decreases monotonically to zero.

Likewise for the piecewise-linear shear layer, as the stratification increases, the wavenumber of the most unstable mode increases only moderately from its unstratified value as represented by $\tilde{k} \simeq 0.40$ and the frequency, with respect to the flow at the centre of the shear layer, is zero.

We now consider the circumstance in which the fluid is nonuniformly stratified. In particular, we consider a piecewise-linear shear layer, represented by eqn (26), in a stratified fluid represented by

$$N^2 = \begin{cases} {N_1}^2 & z \geq H + L \\ {N_0}^2 & z < H + L. \end{cases} \tag{35}$$

Equivalently, the stratification can be represented by the bulk Richardson numbers $J_0 \equiv [N_0/(U_0/L)]^2$ and $J_1 \equiv [N_1/(U_0/L)]^2$, representing the stratification within and above the shear layer, respectively.

In the particular case $J_0 = 0$, the stability characteristics could be assessed as above in a mechanical fashion. However, the resulting eigenvalue problem results in finding the roots of a quintic polynomial in $\tilde{\omega}$.

Rather than considering asymptotic solutions of this problem, here we intuit the nature of the solutions in problems by way of comparing our solutions for the unstratified KH instability and the RI instability problems discussed above. Specifically we wish to determine under what circumstances internal waves are generated as a result of linear instability.

First suppose $J_0 = 0$. If J_1, the growth rate of the most unstable RI mode is larger than the growth rate for KH modes. However, for $J_1 < 1/4$, the frequency of the RI mode is larger than N_1 and therefore vertically propagating internal waves are not directly excited.

If J_1 is large, the growth rate of the KH mode is larger than that for the most unstable RI mode. Explicitly, this occurs if $J_1 > 1/(8 \times 0.20)^2 \simeq 0.39$. Over this range of J_1 the Doppler-shifted frequency of the KH mode is less than the buoyancy frequency above $z = H$ and so we expect internal waves should be directly excited by KH instability. The corresponding wavenumber is given by $\tilde{k}^\star \equiv k^\star L \simeq 0.40$. Comparing this with the wavenumber of the most unstable RI mode, given by $\hat{k}^\star \equiv k^\star H \simeq 0.35$, we expect the strongest resonant coupling between KH and RI modes should occur if $H/L \simeq 0.88$ and $J_1 \gtrsim 0.39$.

For intermediate J_1 (between approximately 1/4 and 0.39) we might hypothesize that internal waves are generated by RI rather than KH instability. However, the asymptotic approximations given by eqns. (33) and (34) do not extend well into this range. It is also unclear whether the nonlinear development of RI instability would suppress the growth of KH instability or whether the two modes would grow in tandem, both generating internal waves with different wavenumbers and frequencies. Nonlinear numerical simulations could give insight into these dynamics, but study of them is beyond the scope of the work presented here.

Finally, we consider the effect of increasing N_0. This would decrease the growth rate of both the KH and RI modes but the frequency would vary only weakly. Thus we expect our conclusions above will not be significantly altered. In particular, we expect internal wave generation by dynamic instability if $J_0 \leq 1/4$ and $J_1 \geq (\tilde{k}^\star)^2 \simeq 0.16$. The latter condition results from the requirement that the Doppler-shifted frequency of propagating internal waves must be less than the ambient buoyancy frequency.

4 Numerical simulations

Linear theory usefully predicts the scale and frequency of modes that one expects will develop in an unstable flow. It can also predict under what circumstances internal waves are dynamically generated in a nonuniformly stratified shear flow. However, fully nonlinear simulations are necessary to determine whether internal waves continue to be excited after the modes grow to large amplitude. We will show below that this is indeed the case and that the momentum extracted from the shear by the waves is so large that the evolution of the shear is significantly modified.

4.1 The model

We solve the fully nonlinear, Boussinesq equations of motion in two-dimensions using a mixed finite-difference, spectral code. So that the calculation remains numerically stable, we include terms representing the diffusion of momentum and density, but we set the associated Reynolds and Schmidt numbers sufficiently large (both approximately 1000 based on the shear strength and depth) so that diffusion effects do not dominate the dynamics. The details of this model are described by Sutherland [11].

The code is initialised with a background velocity profile given by eqn. (26) and with a continuous background density profile corresponding to the stratification given by eqn. (35). The values are prescribed in nondimensional units by setting $L = 1$ and $U_0 = 1$. Thus length-scales are measured as multiples of the shear half-depth and time-scales are measured as multiples of the inverse shear L/U_0. The system is thereby characterised by three independent nondimensional parameters: J_0, J_1 and $\delta \equiv H/L$. Here we will restrict $J_0 = 0.01$ and examine the effect of varying J_1 and δ alone.

In all simulations the domain is bounded vertically by flat, free-slip boundaries at $z = -40$ and 100 (in nondimensional units). The (periodic) horizontal extent of the domain is set to accommodate one wavelength of the most unstable mode. We are interested primarily in internal wave generation from KH instability, so we set the extent to be $L_x = 2\pi/0.41 \simeq 15.3$, in which $k^\star \simeq 0.41$ is the wavenumber of the mode unstable KH mode. This is determined by a Galerkin analysis that includes the effects of diffusion on the growth of the most unstable mode. The fact that the growth rate and wavelength of the most unstable mode are comparable to those predicted by inviscid linear theory is confirmation that diffusion does not play a significant role in the observed dynamics. Even with δ small, our linear stability analysis predicts that the wavenumber of the most unstable RI mode differs from that of the KH mode by a small percentage if $J_1 \gtrsim 0.25$. So we keep L_x fixed in all simulations. The most unstable mode is superimposed on the background flow with its amplitude set so that its maximum vertical velocity is initially 0.01. We superimpose small-amplitude noise in higher modes.

During the flow evolution, the fields of vorticity, ζ, and perturbation density, ρ, are periodically extracted. These serve to illustrate how the structure of the shear layer evolves and to reveal the generation and propagation of internal waves. We further compute the vertical profiles of the horizontally averaged horizontal velocity $\langle u \rangle$ and the approximate wave-induced mean flow computed in terms of the horizontal average $\langle \zeta\xi \rangle$, in which ξ is the vertical displacement field.

4.2 Qualitative results

Figure 2 shows the evolution of a piecewise linear shear layer in uniformly stratified fluid with $J_1 = J_0 = 0.01$ at (nondimensional) time $t = 100$. The two leftmost panels show snapshots of the vorticity field, ζ and the normalised perturbation density field, $\tilde{\rho} = \rho/(-\bar{\rho}'(0))$.

$\tilde{\rho}$ is equivalent to the vertical displacement field, ξ.

The vorticity field is dominated by a well-developed vortex of negative sign. Movies of the simulation reveal that the centre of the vortex remains stationary throughout the flow evolution. Additional baroclinically generated vorticity of positive and negative sign develops on either flank of this coherent structure due to the vertical displacement of stratified fluid in the mixing region.

The perturbation density field shows that fluid is displaced above and below the vortex and, more importantly, internal waves are not evident above or below the mixing region.

Figure 2b compares the mean horizontal flow at time $t = 100$ with the initial mean flow. The nonlinear growth of the instability and consequent evolution has the effect of redistributing the momentum about $z = 0$ so that the maximum shear is approximately half its initial strength. The half-depth of the resulting shear layer after adjustment widens by approximately 3δ. Figure 2c shows that mixing locally reduces the stratification at the centre of the shear layer, and more strongly stratified regions develop above and below the shear.

Transport diagnostics are shown in Figures 2e and f. The former plots the wave-induced mean flow profile. The maximum value of this field is less than 0.4 percent of the background flow speed above $z = 5$, demonstrating that wave-wave interactions negligibly affect the mean flow profile. The latter plots the Reynolds stress per unit mass. The symmetric structure reflects how the mixing region redistributes momentum about the shear layer, but negligible momentum is transported away from the mixing region.

In nonuniformly stratified fluid, the evolution of the flow can be qualitatively different. For example, Figure 3 shows the results of a simulation with a piecewise linear shear in stratified fluid characterised by eqn. (35) with $J_0 = 0.01$, $J_1 = 1.0$ and $\delta = 3$. Thus the stratified region is situated 4δ above the midpoint of the initial shear layer (approximately the half-width of the mixed region in the uniformly stratified case considered above).

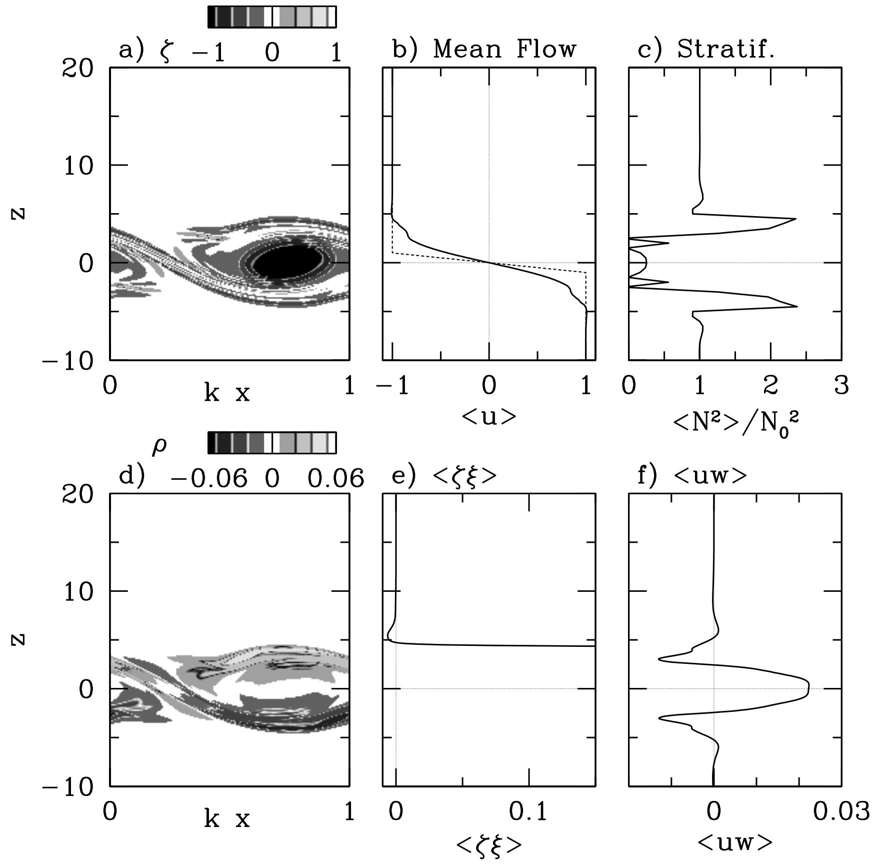

Figure 2: Diagnostics at time $t = 100$ from simulated evolution of piecewise-linear shear in constant stratification $J_0 = 0.01$. a) Vorticity field ζ, b) mean horizontal flow at $t = 0$ (dashed line) and at $t = 100$ (solid line), c) squared buoyancy frequency normalised by initial buoyancy frequency at $z = 0$, d) normalised perturbation density field ρ, e) wave-induced mean flow profile, and f) Reynolds stress per unit mass.

Most striking in these images is the vertical propagation of internal waves above the shear layer visualised by the diagonal bands in both the vorticity and perturbation density fields. Unlike the case with uniform stratification, here the perturbation density field is negligibly small in the mixing region. Furthermore, the coherent vortex is shifted to the left and is displaced downward from the position of its counterpart in Figure 2a. Indeed, movies of the simulation reveal that the vortex in Figure 3a moves steadily from left to right. This occurs because the internal waves extract significant momentum

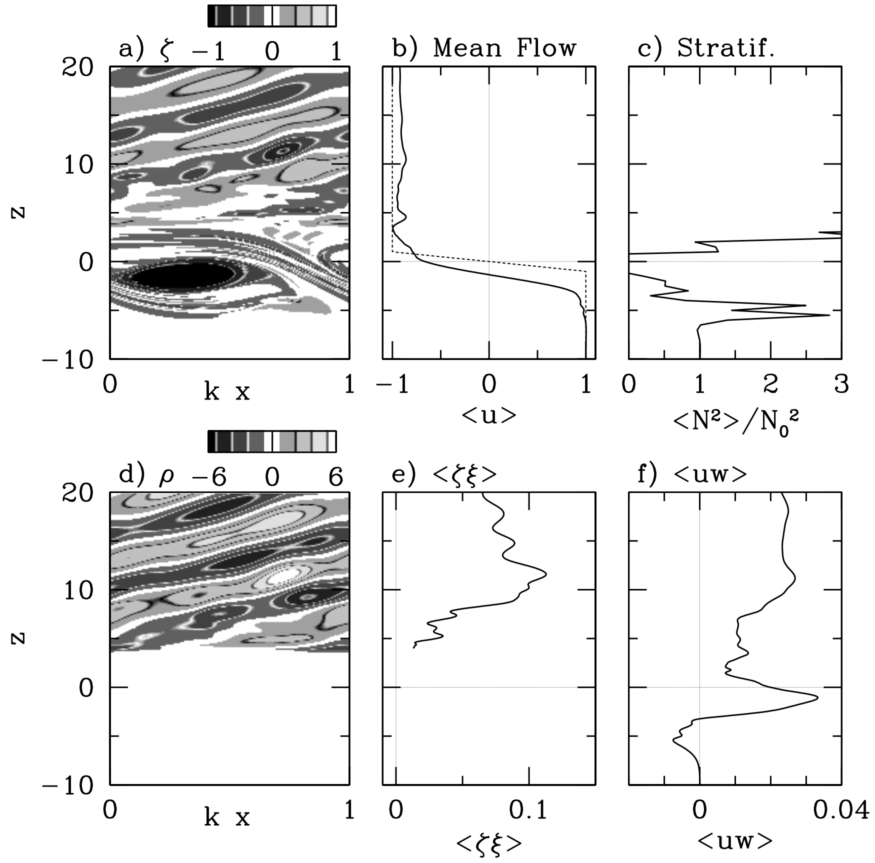

Figure 3: As in Fig. 2 but for simulation with stratification $J_0 = 0.01$ below $z = 4\delta$ and $J_1 = 1$ above $z = 4\delta$.

from the mixing region effectively resulting in a drag to the mean flow.

When internal waves are generated, the mean flow profile is not symmetric about $z = 0$ but instead exhibits significant increases to the initial flow well above the shear layer. Above $z = 1 + \delta$, these increases are equivalent to the wave-induced mean flow (Figure 3e), which is as large as 10 percent of the background flow speed. Likewise the Reynolds stress per unit mass (Figure 3f) is substantial well above the mixing region.

Rather than retard mixing, Figure 3c shows that mixing is more efficient near $z = 0$ where the density gradient is uniform. Above $z = 1 + \delta$, N^2 is perturbed by as much as 2 percent of its mean value (though this is not shown in the plot because N^2 holds values two orders of magnitude larger than the scale shown for $z > \delta$.).

If the stratified region lies in even closer proximity to the shear layer, the

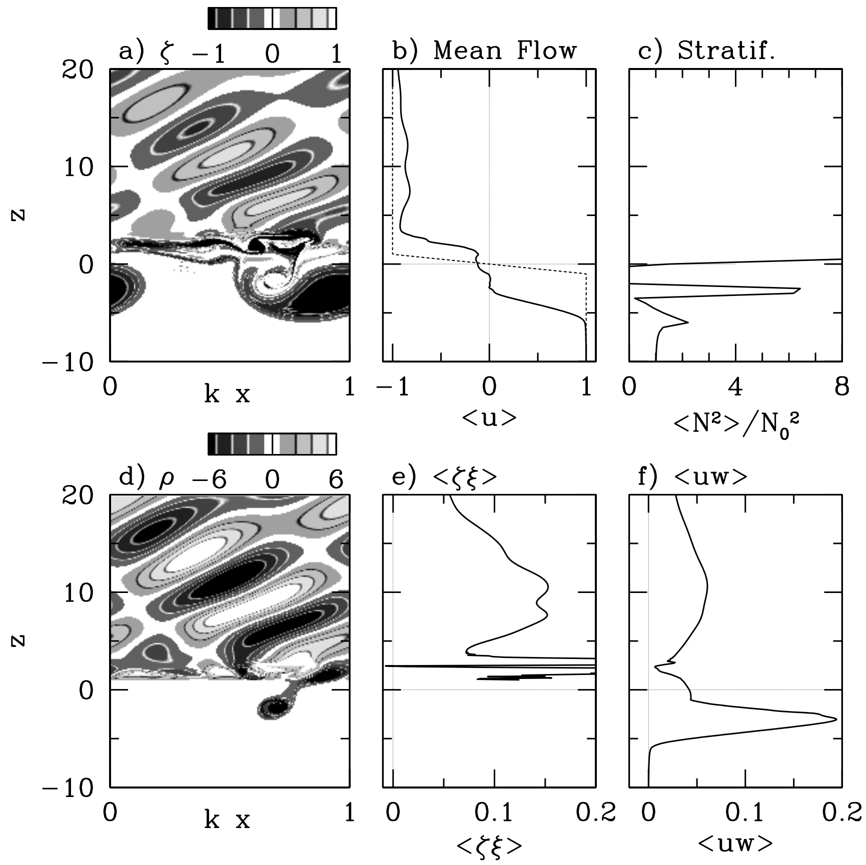

Figure 4: As in Fig. 2 but for simulation with stratification $J_0 = 0.01$ below $z = \delta$ and $J_1 = 1$ above $z = \delta$.

vortex that would develop in uniformly stratified shear is inhibited from penetrating into the stratified region. However, as shown in Figure 4, even in the case $\delta = 0$ significant internal wave generation occurs.

A striking difference between simulations with $\delta = 3$ and $\delta = 0$ is the magnitude of the Reynolds stress per unit mass that, in the latter case, is five times larger in the mixing region. The internal wave radiation is also larger resulting from efficient coupling with the mixing region.

During the initial stages of the flow development, we might expect strong coupling between the shear and internal waves through RI instability. At well-developed times a vortex develops nonetheless as a result of (weaker) KH instability. Internal wave transmission continues to be strong at these late times because the vortex draws dense fluid downward into the mixing region. Rather than convectively disrupting the coherent vortex, the buoyant fluid seems rather to push the vortex upward against the stratified region. The resulting vertical pertubation to the base of the stratified region that translates horizontally excites internal waves in a manner similar to wave generation by stratified flow over topography.

4.3 Quantitative results

We quantify the effect of internal wave transmission on the evolution of the mixing region by assessing the momentum transported by waves and the consequent displacement and spreading of the mean flow.

Typically, momentum transport is represented by the Reynolds stress $\tau = \rho_0 \langle uw \rangle$, which measures the vertical transport of horizontal momentum and, consequently, the drag imparted to the mean flow. This connection is revealed by the horizontally averaged horizontal momentum equation for inviscid, Boussinesq flow:

$$\frac{\partial \langle \rho_0 u \rangle}{\partial t} = -\frac{\partial \tau}{\partial z}. \tag{36}$$

The average decrease in the momentum of the mean flow between two fixed levels, z_1 and z_0, respectively above and below the mixing region, can be computed by finding the integral over time of $\tau(z_1) - \tau(z_0)$ and dividing by $z_1 - z_0$.

Here we take an alternative route to the same result. At a fixed time we measure the approximate vertical profile of the wave-induced mean flow, $\langle \zeta\xi \rangle$. To second order accuracy in amplitude, this quantity approximately equals the pseudomomentum per unit mass of internal waves [21, 22, 23]. Integrating vertically gives the loss of momentum per unit mass to the mean flow by wave momentum transport, $\Delta M = \int \langle \zeta\xi \rangle \, dz$. This quantity may instead be represented by $\left\langle \Delta z_{\mathrm{igw}} \right\rangle = \Delta M / 2U_0$, which characterises the equivalent depth of the shear layer that has the same structure as the initial shear layer, $\bar{U}(z)$, but that has translated downward due to the momentum loss so that it has the form $\bar{U}(z + \left\langle \Delta z_{\mathrm{igw}} \right\rangle)$.

The difference between vertical profiles of the horizontally averaged flow $\langle u \rangle$ and of $\langle \zeta\xi \rangle$ reveals how momentum has been redistributed due to mixing. We quantify this redistribution by computing the mean, μ_u, and standard deviation, σ_u, of the background shear, $d \langle u \rangle / dz$, both initially and at time t_a. The difference between the means gives the relative change in height of the mean flow, $\langle \Delta z_{\mathrm{shr}} \rangle$. The difference of the standard deviations gives the relative increase in the depth of the shear layer. The latter difference is normalised by $\sigma_u|_{t=0}$ to give $\Delta\sigma$. This measures the spread of the mixing region relative to the half depth of the initial shear.

We have performed this analysis at $t_a = 100$ being a sufficiently long time for the mixing region to be well developed and for internal waves, if they are generated, to extract significant momentum from the mean flow.

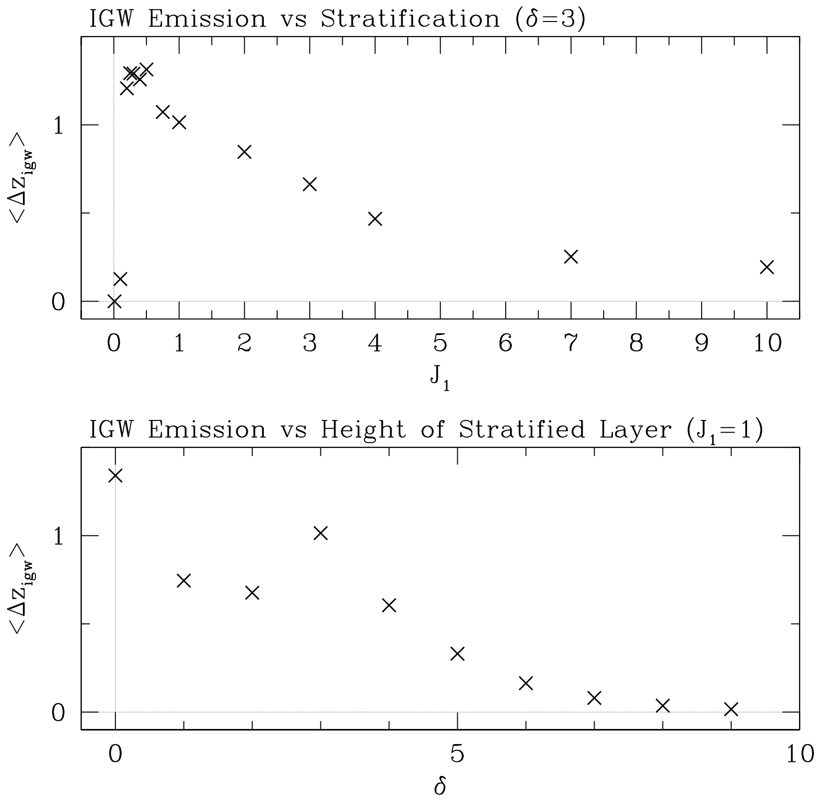

Figure 5: Loss of momentum per unit mass due to internal wave emission, ΔM, as a function of a) J_1, the stratification above the shear and b) the relative height, δ, of the region with increased stratification above the shear. The points in a) are computed with $\delta = 4$. The points in b) are computed with $J_1 = 1$.

Figure 5 shows values of ΔM computed from simulations with a range of values of J_1 and δ. In Figure 5a, for which we fix $\delta = 3$, we find that the momentum extraction by waves is small for $J_1 \lesssim 0.1$, increases dramatically for $0.2 \lesssim J_1 \lesssim 0.5$, and gradually decreases thereafter. Analysis of the power spectra of the waves (not shown) reveals that the magnitude of the ratio of the vertical to horizontal wavenumber increases approximately as the square root of J_1 as J_1 becomes large. This is consistent with linear theory for waves with fixed horizontal wavenumber and frequency.

Figure 5b shows that the proximity of the region of increased stratification to the shear layer is a crucial parameter in determining wave transmission.

In simulations with $J_1 = 1$, transmission is greatest when the stratified layer immediately overlies the shear layer ($\delta = 0$). As δ increases, transmission decreases until $\delta \simeq 3$ at which point transmission rapidly increases again. This jump occurs as the instability mechanism switches from direct coupling with internal waves through RI instability to indirect coupling through KH instability. For still larger δ transmission decreases until $\delta \gtrsim 9$ in which case transmission is negligibly small.

The impact of wave transmission upon the evolution of the mixing region is examined in Figure 6. In the control simulation with $J_1 = J_0 = 0.01$, $\langle \Delta z_{\rm shr} \rangle = 4 \times 10^{-4}$ and $\Delta\sigma = 0.6$. This negligible mean and small standard deviation indicates that mixing acts only moderately to redistribute momentum about the initial region of maximum shear. In simulations with $\delta = 3$ (Figure 6a), we find the width of the shear layer widens moderately and the mean depth of the shear layer decreases as a consequence of wave transmission with $0.2 \lesssim J_1 \lesssim 0.5$. For larger J_1, the mean depth of the shear changes less from its initial position. However the extent of the mixing region increases dramatically. This occurs because the mixing region entrains more dense fluid as J_1 increases and this results in convection, though less efficient wave transmission.

For fixed J_1, Figure 6b shows that the width of the mixing region increases for $0 \lesssim \delta \lesssim 2$, then rapidly changes to a smaller width and to a mean depth that is moderately smaller. Thus, whereas RI instability enhances mixing, coupling between internal waves and KH instability acts primarily to displace the mean depth of the shear layer through extraction of momentum, but does not act to enhance mixing.

5 Conclusion

We have reviewed linear theory examining the stability of stratified shear flow and have explored a new mechanism for internal wave excitation through Rayleigh - internal wave coupling in non-uniformly stratified fluid. Fully nonlinear numerical simulations reveal that this mechanism is indeed efficient at generating waves well beyond the linear regime. For a shear layer with half depth L and speeds $\pm U_0$ on either flank of the shear, internal waves are continuously excited over the time $t = 100L/U_0$ of the simulations presented here with $0.2\,(U_0/L)^2 \lesssim {N_1}^2 \lesssim 10\,(U_0/L)^2$ and $0 \leq H \lesssim 9L$.

Internal wave excitation is strongest if ${N_1}^2 \simeq 0.5\,(\pm 0.25)\,U_0/L$. In this case waves are excited with frequencies, $\Omega = U_0 k \simeq 0.4\,U_0/L$, close to but smaller than the buoyancy frequency, N_1. From the dispersion relation given by eqn. (15), but replacing N_0 with N_1, the angle of phase lines of these nonhydrostatic waves lies between 37^o and 62^o.

The work presented here is limited in two important ways. First, the simulations, being restricted to two dimensions, are unrealistic for long times. Spanwise disturbances to Kelvin-Helmholtz vortices and braids between

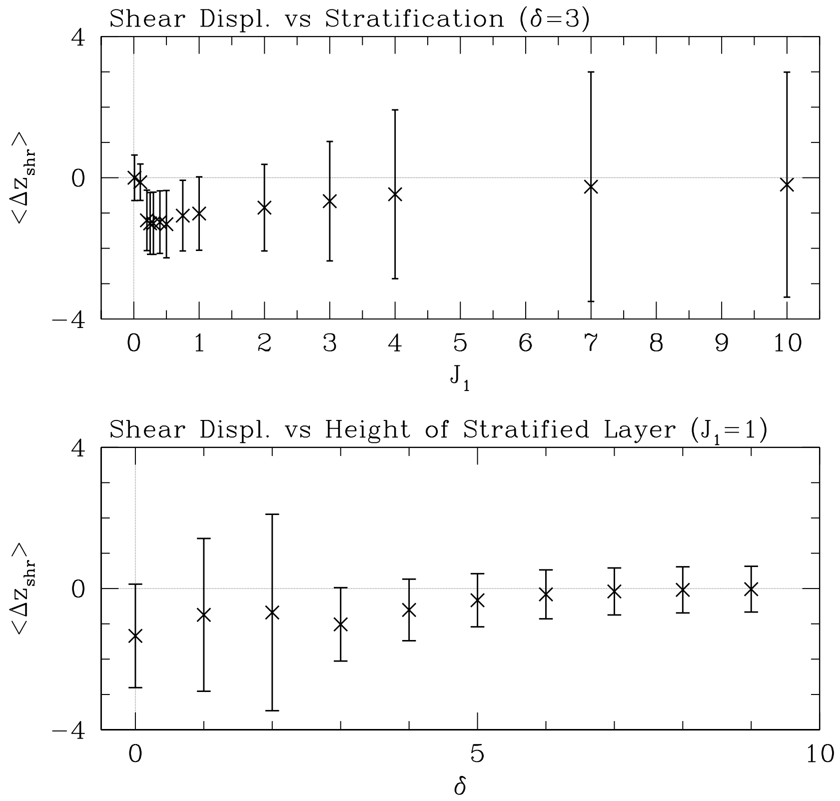

Figure 6: As in Fig. 5 but showing the displacement, $\langle \Delta z_{\rm shr} \rangle$ (crosses), and the spread, $\Delta\sigma$ (vertical bars), of the mixing region as a function of a) J_1 and b) δ.

them are known to rapidly result in the turbulent breakdown of this coherent structure [2]. Fully three-dimensional simulations should be performed to investigate the coupling between internal waves and this sheared turbulent region. Despite the fast time-scales involved in turbulence, significant internal wave generation is still anticipated on the basis of recent laboratory experiments of wave generation in an unsheared turbulent mixing region [24].

A second limitation is the applicability of this work to realisable flows. Most observations indicate that mean shear is strongest in regions of large, not small, density gradients. However, some large-scale geophysical flows have structures close to the conditions we have examined. For example, the upper flank of the jet stream at the tropopause underlies the stratosphere. Observations suggest that internal wave transmission may be associated with perturbations to the jet stream [25, 26, 27], though it is unclear whether this is through the dynamic instability mechanism we have examined here, through envelope radiation, or through mixed-region collapse. The equatorial undercurrent may be another example of realisable dynamic instability. The upper flank of this current lies in the proximity of the mixed region with an underlying strongly stratified thermocline. Significant turbulence and internal wave activity have been observed near the current [28, 29]. Although mechanisms for dynamic excitation have been explored [10, 13], more observations are required to determine the relative importance of this process compared with other wave-generation mechanisms.

Acknowledgements

This research was supported by the Canadian Foundation for Climate and Atmospheric Science (CFCAS).

References

[1] Smyth, W.D. & Peltier, W.R., The transition between Kelvin-Helmholtz and Holmboe instability: An investigation of the overreflection hypothesis. *J Atmos Sci*, **46(24)**, pp. 3698–3720, 1989.

[2] Peltier, W.R. & Caulfield, C.P., Mixing efficiency in stratified shear flows. *Annu Rev Fluid Mech*, **35**, pp. 135–167, 2003.

[3] Lindzen, R.S., Stability of a Helmholtz velocity profile in a continuously stratified infinite Boussinesq fluid – applications to clear air turbulence. *J Atmos Sci*, **31**, pp. 1507–1514, 1974.

[4] Lindzen, R.S. & Rosenthal, A.J., On the instability of Helmholtz velocity profiles in stably stratified fluids when a lower boundary is present. *J Geophys Res*, **81(9)**, pp. 1561–1571, 1976.

[5] Fritts, D.C., Shear excitation of atmospheric gravity waves. Part II: Nonlinear radiation from a free shear layer. *J Atmos Sci*, **41(4)**, pp. 524–537, 1984.

[6] Chimonas, G. & Grant, J.R., Shear excitation of gravity waves. Part II: Upscale scattering from Kelvin-Helmholtz waves. *J Atmos Sci*, **41(15)**, pp. 2278–2288, 1984.

[7] Scinocca, J.F. & Ford, R., The nonlinear forcing of large-scale internal gravity waves by stratified shear instability. *J Atmos Sci*, **57**, pp. 653–672, 2000.

[8] Bühler, O., McIntyre, M.E. & Scinocca, J.F., On shear-generated gravity waves that reach the mesosphere, Part I. Wave generation. *J Atmos Sci*, **56**, pp. 3749–3763, 1999.

[9] Sutherland, B.R., Caulfield, C.P. & Peltier, W.R., Internal wave generation and hydrodynamic instability. *J Atmos Sci*, **51**, pp. 3261–3280, 1994.

[10] Sutherland, B.R., The dynamic excitation of internal gravity waves in the equatorial oceans. *J Phys Oceanogr*, **26**, pp. 3214–3235, 1996.

[11] Sutherland, B.R. & Peltier, W.R., Turbulence transition and internal wave generation in density stratified jets. *Phys Fluids A*, **6**, pp. 1267–1284, 1994.

[12] Tse, K.L., Mahalov, A., Nicolaenko, B. & Fernando, H.J.S., Quasi-equilibrium dynamics of shear-stratified turbulence in a model tropospheric jet. *J Fluid Mech*, **496**, pp. 73–103, 2003.

[13] Smyth, W.D. & Moum, J.N., Shear instability and gravity wave saturation in an asymmetrically stratified jet. *Dyn Atmos Oceans*, **35(3)**, pp. 265–294, 2002.

[14] Gill, A.E., *Atmosphere-Ocean dynamics*. Academic Press: San Diego, p. 662, 1982.

[15] Spiegel, E.A. & Veronis, G., On the Boussinesq approximation for a compressible fluid. *Astrophys J*, **131**, pp. 442–447, 1960.

[16] Drazin, P.G. & Reid, W.H., *Hydrodynamic Stability*. Cambridge University Press: Cambridge, England, p. 525, 1981.

[17] Miles, J.W., On the stability of heterogeneous shear flows. *J Fluid Mech*, **10**, pp. 496–508, 1961.

[18] Howard, L.N., Note on a paper by John W. Miles. *J Fluid Mech*, **10**, pp. 509–512, 1961.

[19] Drazin, P.G. & Howard, L.N., Hydrodynamic stability of parallel flow of inviscid fluid. *Advances in Applied Mathematics*, **9**, pp. 1–89, 1966.

[20] Drazin, P.G., The stability of a shear layer in an unbounded heterogeneous inviscid fluid. *J Fluid Mech*, **4**, pp. 214–224, 1958.

[21] Scinocca, J.F. & Shepherd, T.G., Nonlinear wave-activity conservation laws and Hamiltonian structure for the two-dimensional anelastic equations. *J Atmos Sci*, **49**, pp. 5–27, 1992.

[22] Sutherland, B.R., Internal gravity wave radiation into weakly stratified fluid. *Phys Fluids*, **8**, pp. 430–441, 1996.

[23] Sutherland, B.R., Propagation and reflection of large amplitude internal gravity waves. *Phys Fluids*, **11**, pp. 1081–1090, 1999.

[24] Dohan, K. & Sutherland, B.R., Internal waves generated from a turbulent mixed region. *Phys Fluids*, **15**, pp. 488–498, 2003.

[25] Herron, T.J. & Tolstoy, I., Tracking jet stream winds from ground level pressure signals. *J Atmos Sci*, **26**, pp. 266–269, 1969.

[26] Keliher, T.E., The occurrence of microbarograph-detected gravity waves compared with the existence of dynamically unstable wind shear layers. *J Geophys Res*, **80**, pp. 2967–2976, 1975.

[27] Fritts, D.C. & Nastrom, G.D., Sources of mesoscale variability of gravity waves. Part II: Frontal, convective, and jet stream excitation. *J Atmos Sci*, **49**, pp. 111–127, 1992.

[28] Moum, J.N., Caldwell, D.R. & Paulson, C.A., Mixing in the equatorial surface layer and thermocline. *J Geophys Res*, **94**, pp. 2005–2021, 1989.

[29] Peters, H., Gregg, M.C. & Toole, J., Meridional variability of turbulence through the equatorial undercurrent. *J Geophys Res*, **94**, pp. 18003–18009, 1989.